Acta Crystallographica Section D
Biological Crystallography
ISSN 0907-4449

Structural characterization of V57D and V57P mutants of human cystatin C, an amyloidogenic protein

Marta Orlikowska,[a] Aneta Szymańska,[a] Dominika Borek,[b] Zbyszek Otwinowski,[b] Piotr Skowron[c] and Elżbieta Jankowska[a]*

[a]Department of Medicinal Chemistry, Faculty of Chemistry, University of Gdansk, Sobieskiego 18/19, 80-952 Gdansk, Poland, [b]Department of Biochemistry, University of Texas Southwestern Medical Center, 5323 Harry Hines Boulevard, Dallas, TX 75390-8816, USA, and [c]Division of Environmental Molecular Biotechnology, Faculty of Chemistry, University of Gdansk, Sobieskiego 18/19, 80-952 Gdansk, Poland

Correspondence e-mail: elaj@chem.univ.gda.pl

Received 5 October 2012
Accepted 21 December 2012

PDB References: human cystatin C, V57P mutant, 3s67; V57D mutant, 3sva

Wild-type human cystatin C (hCC wt) is a low-molecular-mass protein (120 amino-acid residues, 13 343 Da) that is found in all nucleated cells. Physiologically, it functions as a potent regulator of cysteine protease activity. While the biologically active hCC wt is a monomeric protein, all crystallization efforts to date have resulted in a three-dimensional domain-swapped dimeric structure. In the recently published structure of a mutated hCC, the monomeric fold was preserved by a stabilization of the conformationally constrained loop L1 caused by a single amino-acid substitution: Val57Asn. Additional hCC mutants were obtained in order to elucidate the relationship between the stability of the L1 loop and the propensity of human cystatin C to dimerize. In one mutant Val57 was substituted by an aspartic acid residue, which is favoured in β-turns, and in the second mutant proline, a residue known for broadening turns, was substituted for the same Val57. Here, 2.26 and 3.0 Å resolution crystal structures of the V57D andV57P mutants of hCC are reported and their dimeric architecture is discussed in terms of the stabilization and destabilization effects of the introduced mutations.

1. Introduction

A wide range of human pathologies are associated with the formation of amyloid fibrils through the aggregation of polypeptide chains; among them are Alzheimer's and Parkinson's diseases (Chiti & Dobson, 2006). Results from multiple studies suggest that the conversion of soluble proteins into insoluble amyloid fibrils may involve three-dimensional domain swapping of structural elements.

The term 'three-dimensional domain swapping' was introduced in 1994 to describe a dimeric structure of diphtheria toxin (Bennett *et al.*, 1994, 1995). However, it had been known much earlier that a process existed by which identical structural elements could be exchanged between two monomers, resulting in the formation of an intertwined dimer. This was proposed for the first time in 1962 to explain the behaviour of mutated RNase A (Crestfield *et al.*, 1962). Since then, this phenomenon has been observed in approximately 60 different proteins (Liu *et al.*, 2011) that have been studied by X-ray crystallography. They are reported in the 3Dswap knowledgebase, which gathers proteins involved in three-dimensional domain swapping (Shameer *et al.*, 2011; http://caps.ncbs.res.in/3dswap). Analyses of these structures indicated that a protein can swap either an entire subdomain or, more frequently, only a simple secondary-structure element such as an α-helix or β-sheet. The lack of size restrictions as well as any requirements or preferences for specific sequence or structure motifs

in the interchanged domains suggests that under appropriate conditions swapping may take place in any protein with an unconstrained terminus (Liu & Eisenberg, 2002).

Human cystatin C (hCC) is an example of a protein that dimerizes through three-dimensional domain swapping (Janowski *et al.*, 2001). It belongs to a family of natural inhibitors of papain-like and legumain-related cysteine proteases which control protein turnover and serve as a defence against invasion by parasites and viruses (Barrett, 1987). Cystatins have also been implicated in amyloid and neurodegenerative diseases (Žerovnik *et al.*, 2011). The L68Q variant of human cystatin C, found endemically in the Icelandic population, is the causative agent of an amyloidogenic disease, hereditary cystatin C amyloid angiopathy, in which repeated haemorrhage, dementia, paralysis and eventual death of young adults are associated with cystatin deposits in cerebral blood vessels (Olafsson & Grubb, 2000).

Although wild-type hCC (hCC wt) is a monomeric protein under physiological conditions, there are reports of the co-deposition of hCC wt with amyloid β in parenchymal and vascular plaques in the brains of Alzheimer's disease patients (Sastre *et al.*, 2004). This suggests that the wild-type protein may also participate in amyloid-fibril formation.

The mechanism of cystatin C fibrillization has not been fully elucidated; nevertheless, the connection between fibrillization and domain swapping was clearly demonstrated when abrogation of hCC domain-swapping dimerization suppressed the formation of hCC fibrils (Nilsson *et al.*, 2004).

Dimerization of hCC wt can be enforced *in vitro* by environmental conditions such as elevated temperature, low pH or the application of mild chemical denaturants (Ekiel & Abrahamson, 1996). During crystallization, high concentrations of hCC also resulted in dimerization (Janowski *et al.*, 2001, 2004, 2005). Dimers of hCC wt created through three-dimensional domain swapping duplicate the protein monomeric fold, which consists of five β-strands wrapped around a central α-helix (Janowski *et al.*, 2001). This dimerization results in loss of the inhibitory activity of hCC against papain-like proteases owing to sequestration of one element of the inhibitory epitope, the L1 loop (55–59; QIVAG), within the dimer interface. The L1 loop serves as a hinge region linking the swapping unit (the α-helix and the two β-strands flanking it) to the rest of the protein molecule. This hinge region is the only part of the hCC chain that changes structurally during the dimerization process, during which it is converted from a loop to part of a long β-strand.

According to experimental (Engh *et al.*, 1993; Martin *et al.*, 1995) and theoretical (Dehouck *et al.*, 2003; Rodziewicz-Motowidło *et al.*, 2009) studies, the dimerization of hCC molecules is driven by conformational constraints attributed to the Val residue (Val57) located at the apex of the L1 loop. The values of the main-chain torsion angles for this residue in the monomeric protein are not optimal (the ψ values for different conformations obtained in MD calculations cluster around 0°) and this may account for the propensity of the protein to undergo domain swapping. We have designed, expressed and purified hCC variants with Val57 mutated either to an Asn, an Asp or a Pro residue. Asn and Asp residues are well recognized as β-turn stabilizers and, as such, are favoured in loop regions. We expected that they would stabilize the hinge loop and shift the equilibrium towards the monomeric fold. A proline residue is frequently present in hinge loops and seems to play a role in modulating the domain-swapping propensity of some proteins (Rousseau *et al.*, 2001). We introduced a proline at position 57 to broaden the turn and test whether this enhances the propensity of hCC for domain swapping.

Dimerization studies performed *in vitro* confirmed our hypothesis. The stabilized hCC variants (V57D and V57N), although structurally and physicochemically very similar to the wild-type protein, exhibited high resistance against dimerization (Szymańska *et al.*, 2009) and subsequent fibrillization (Szymańska *et al.*, 2008). On the other hand, the Pro mutant dimerized easily, probably during expression, and displayed a higher aggregation rate. All of the studied variants retained inhibitory activity towards papain, although to different degrees. In the case of hCC V57N and the monomeric fraction of V57P, which was separated from the dimeric fraction by size-exclusion chromatography, the activity was similar to that measured for wild-type hCC. However, introduction of the charged aspartic acid residue into the inhibitory L1 loop decreased the activity of the protein by about fourfold (Szymańska *et al.*, 2012).

The previously described structure of the V57N mutant of hCC (PDB entry 3nx0; Orlikowska, Jankowska, Kolodziejczyk *et al.*, 2011) is stable in the monomeric form. In this paper, we describe the dimeric structures of the domain-swapped V57P and V57D mutants of human cystatin C, compare them with other forms of hCC and discuss the ability of a residue with a polar, a charged or a constrained side chain to act as a conformational gatekeeper that influences the balance between the monomeric and the dimeric forms.

2. Materials and methods

2.1. Circular dichroism

Circular-dichroism (CD) spectra were collected at room temperature using a Jasco J-815 spectrometer in the range 185–260 nm. Measurements were performed using solutions consisting of 0.3 mg ml^{-1} protein in 0.02 *M* phosphate buffer pH 6.7. For each protein, the results presented constitute an average of two independent measurements.

2.2. Protein crystallization

Protein expression, purification and preliminary crystallization experiments have been described previously for the V57D and V57P hCC variants (Orlikowska, Jankowska, Borek *et al.*, 2011).

A protein solution at a concentration of 10 mg ml^{-1} in water was used in all crystallization experiments. Initial screening for crystallization conditions for the V57D mutant was performed using the commercially available screen The Classics Suite (Qiagen). The conditions were further

Table 1
Data-collection and structure-refinement statistics.

Values in parentheses are for the highest resolution shell.

	hCC V57D (PDB entry 3sva)	hCC V57P (PDB entry 3s67)
Data collection		
Space group	*I*432	*I*432
Unit-cell parameter (Å)	a = 140.14	a = 140.13
Temperature (K)	100	100
Wavelength (Å)	0.97923	0.97923
Resolution (Å)	3.00 (3.05–3.00)	2.26 (2.30–2.26)
Reflections collected	110993	427010
Unique reflections	5422	11315
$R_{\rm merge}$† (%)	0.130 (N/A‡)	0.088 (N/A)
$R_{\rm meas}$§ (%)	0.136 (N/A)	0.091 (N/A)
$\langle I\rangle/\langle\sigma(I)\rangle$	24.9 (2.2)	36.5 (2.16)
Completeness (%)	99.9 (100)	99.8 (100)
Multiplicity	10.9 (11.1)	14.0 (12.5)
Refinement		
Resolution (Å)	3.00	2.26
No. of reflections (work/test set)	5168/247	10697/537
$R_{\rm work}/R_{\rm free}$¶ (%)	20.11/24.19	18.66/22.89
No. of atoms		
Protein	883	872
Water	6	67
Other	11	44
R.m.s.d. from ideal		
Bond lengths (Å)	0.017	0.017
Bond angles (°)	1.620	1.770
Ramachandran statistics (%)		
Most favoured (%)	90.7	95.8
Additionally favoured (%)	9.3	4.2
Generously favoured (%)	0.0	0.0

† $R_{\rm merge} = \sum_{hkl}\sum_i |I_i(hkl) - \langle I(hkl)\rangle| / \sum_{hkl}\sum_i I_i(hkl)$, where $I_i(hkl)$ is the intensity of observation i of reflection hkl. § If $R_{\rm merge}$ exceeds 1.0, *SCALEPACK* does not report its value because it is uninformative. Instead, the $I/\sigma(I)$ criterion is used to define the resolution cutoff. ‡ $R_{\rm meas}$ is the redundancy-independent merging R factor ¶ $R = \sum_{hkl} ||F_{\rm obs}| - |F_{\rm calc}|| / \sum_{hkl} |F_{\rm obs}|$ for all reflections, where $F_{\rm obs}$ and $F_{\rm calc}$ are the observed and calculated structure factors, respectively. $R_{\rm free}$ is calculated analogously for the test reflections, which were randomly selected and excluded from the refinement.

optimized using reagents generated in-house. The crystals used in the diffraction experiment were obtained using a well solution consisting of 0.1 *M* imidazole pH 6.5, 1.0 *M* sodium acetate. The crystals were grown by the vapour-diffusion method in a hanging drop at 293 K using EasyXtal plates (Qiagen). Crystallization drops were prepared by mixing 1 µl protein solution with 1 µl well solution on a cover slide. The drops were equilibrated against 500 µl well solution. The crystals were soaked in reservoir solution supplemented with 30%(*v*/*v*) PEG 400 for cryoprotection and then plunged into liquid nitrogen.

The sample of the V57P hCC mutant used in crystallization trials was not homogenous with regard to the oligomeric state, as it was collected from gel-filtration fractions that contained a monomeric form of the mutant that equilibrated very quickly with a dimer.

The initial crystallization trials for the V57P mutant were performed in a high-throughput mode with a Phoenix robot using the commercially available screens The Classics, PACT and JCSG+ Suites (Qiagen) and Index (Hampton Research). All trials were carried out by the sitting-drop vapour-diffusion method at 293 K in 96-well plates by mixing 200 nl protein solution with 200 nl screen solution and equilibrating the drops against 50 µl well solution. Initial crystals were obtained from condition Nos. 38 (0.1 *M* imidazole pH 6.5, 1.0 *M* sodium acetate) and 40 (0.1 *M* sodium cacodylate pH 6.5, 1.4 *M* sodium acetate) of The Classics Suite. Optimization screens were performed using reagents generated in-house and the commercially available Additive Screen (Hampton Research), which is a library of small molecules that can affect the crystallization of biological macromolecules. Two separate methods of setup were used for the additive screen depending on the volatility of the additives. Nonvolatile additives were only added to the drop (additive, protein and well solution mixed in a 1:5:4 ratio). For volatile additives, the additive was added to the reservoir solution at a 1:9 ratio of additive to reservoir and the well solution was then mixed with the protein solution in a 1:1 ratio in the drop. The best crystals were obtained with a well solution consisting of 0.1 *M* imidazole pH 6.5, 0.9 *M* sodium acetate and were grown using the hanging-drop vapour-diffusion method at 293 K by mixing 2 µl protein solution, 0.4 µl 2.0 *M* additive NDSB-221 [3-(1-methylpiperidinium)-1-propanesulfonate] and 1.6 µl well solution on a cover slide and equilibrating the drop against 500 µl well solution in EasyXtal plates (Qiagen). Before cryocooling in liquid nitrogen, the crystals were transferred into mother liquor supplemented with 30%(*v*/*v*) PEG 400.

For both proteins we also tried the crystallization conditions which had previously led to the monomeric structure of V57N hCC. However, neither V57D nor V57P produced crystals from drops consisting of the protein and well solution (0.1 *M* sodium cacodylate pH 6.5, 0.2 *M* ammonium sulfate, 25% PEG 8000) in a 1:1 ratio.

2.3. Data collection and processing

X-ray diffraction data were collected at 100 K using synchrotron radiation on beamline 19BM of the Advanced Photon Source (APS), Argonne National Laboratory, Chicago at a wavelength of 0.97923 Å with an ADSC Quantum Q210r CCD detector. The data-collection statistics are summarized in Table 1.

For the crystal of the V57D mutant, 180 frames were collected at a crystal-to-detector distance of 290 mm using an oscillation step of 0.5°. Diffraction data were measured to 3.0 Å resolution. A unique data set consisting of 5422 reflections was obtained after merging 110 993 observations. This data set was 99.9% complete (100% complete in the last resolution shell) and was characterized by an $R_{\rm merge}$ of 0.130 and an $\langle I\rangle/\langle\sigma(I)\rangle$ of 24.9.

For the crystals of hCC V57P, 240 frames were collected at a crystal-to-detector distance of 200 mm using an oscillation step of 1.0°. A total of 427 010 reflections were measured and were reduced to 11 315 unique observations extending to 2.26 Å resolution. This data set was 99.8% complete (100% complete in the last resolution shell) and was characterized by an $R_{\rm merge}$ of 0.088 and an $\langle I\rangle/\langle\sigma(I)\rangle$ of 36.5.

The images were indexed, integrated and scaled using the *HKL*-3000 package (Otwinowski & Minor, 1997; Minor *et al.*, 2006).

2.4. Structure determination and refinement

The structures were solved by the molecular-replacement method using *MOLREP* (Vagin & Teplyakov, 2010). Since the crystals of the V57D and V57P mutants were isomorphous to the cubic form of hCC wt, the folding unit of wild-type human cystatin C (PDB entry 1g96; Janowski *et al.*, 2001) was used as a search probe. The model was refined in *REFMAC* (Murshudov *et al.*, 2011) from the *CCP*4 package (Winn *et al.*, 2011). Optimum TLS parameters were analyzed using the *TLS Motion Determination* server (Painter & Merritt, 2006*a*,*b*) and seven and 11 TLS groups were used during refinement for hCC V57D and V57P, respectively. Model rebuilding in the electron-density maps was performed using the program *Coot* (Emsley & Cowtan, 2004). Water and ligand molecules which were present either in the crystallization conditions or in the cryoprotectant solution (PEG) were added manually in *Coot*. A strong peak which was observed in the difference electron-density map ($F_o - F_c$) was assigned as a chloride ion since hydrochloric acid was used to adjust the pH of the crystallization buffers. The final model of V57D contained six water molecules, one acetate ion and one PEG molecule. In the structure of hCC V57P, 67 water molecules, one chloride ion, three acetate ions, two imidazole molecules and three PEG molecules were modelled.

The progress of refinement was monitored and the model was validated using the R_{free} parameter (Brünger, 1992). The quality of the final structure was assessed with *PROCHECK* (Laskowski *et al.*, 1993) and the *MolProbity* server (Chen *et al.*, 2010). The structure-refinement statistics are summarized in Table 1.

Atomic coordinates and displacement parameters, together with structure-factor amplitudes, have been deposited in the RCSB Protein Data Bank under accession codes 3s67 (hCC V57P mutant) and 3sva (hCC V57D mutant). In the PDB entry 3s67 the side chain of Arg70 has been flipped as it evidently has the wrong rotation. Both N^{ε} and $N^{\eta 2}$ should interact with the Asp40 side chain.

3. Results and discussion

3.1. Structure determination

Crystallization trials for the hCC V57P mutant resulted in drops that contained many very small and thin crystals. After testing the most promising conditions (0.1 *M* imidazole pH 6.5, 1.0 *M* sodium acetate) with the commercially available Additive Screen, we obtained crystals that were sufficiently large for data collection. Most of them did not diffract well (resolution above 5 Å) and data indexing performed on these low-resolution diffraction patterns resulted in a high-symmetry space group $P6_x22$ with large unit-cell parameters a = 246, b = 246, c = 375 Å. The values of the Matthews coefficient (between 3.10 and 2.70 Å^3 Da^{-1}) suggest that the asymmetric unit of this crystal form may contain between 40 and 46 copies of the hCC molecule (Orlikowska, Jankowska, Borek *et al.*, 2011). Multiple copies of the molecule in the asymmetric unit, in combination with the detected lower stability of the mutant in its monomeric form (Szymańska *et al.*, 2009; Jankowska *et al.*, 2012), may indicate a propensity for oligomerization that is higher than that of wild-type hCC. However, crystals grown in a solution containing NDSB-221 [3-(1-methylpiperidinium)-1-propanesulfonate] as an additive (up to 0.4 *M*) gave good-quality diffraction data. NDSB is a nondetergent zwitterionic compound that can prevent non-specific interactions in solutions of proteins. When used as a crystallization-drop component, it probably diminished the tendency of V57P towards aggregation. The obtained cubic crystals diffracted to 2.26 Å resolution and had space-group symmetry *I*432. The Matthews coefficient was 4.3 Å^3 Da^{-1}, which corresponds to one molecule per asymmetric unit and 71.5% solvent content. Molecular-replacement calculations returned the perfectly symmetrical domain-swapped dimer as a solution (Fig. 1), with the two polypeptide chains creating it related by a crystallographic twofold rotation. The refinement converged with a final R factor of 18.66% (R_{free} = 22.89%) for all data (Table 1). The final model was characterized by a root-mean-square deviation (r.m.s.d.) from ideal bond lengths of 0.017 Å, with 95.8% of all residues in the most favoured areas of the Ramachandran plot (no residues were found in disallowed regions).

The crystals of hCC V57D diffracted to a resolution of 3.0 Å and had the same cubic symmetry as the V57P mutant. Molecular replacement resulted in a single polypeptide chain in the asymmetric unit which is related by a crystallographic twofold rotation axis to the copy with which it forms the domain-swapped dimer. The dimer is identical to the wild-type and V57P hCC structures (Fig. 1). The refinement converged with a final R factor of 20.11% and an R_{free} of 24.19% (Table 1). The root-mean-square deviation of the final model from the ideal geometry was 0.017 Å for the bond lengths. Excluding glycine and proline residues, the Ramachandran plot had 90.7% of the residues in the most favoured regions and 9.3% of the residues in the additionally allowed regions, with no residues in the disallowed regions.

3.2. Overall fold

The structures of hCC V57D and V57P are shown in Fig. 1. Similar to other proteins from the cystatin family for which

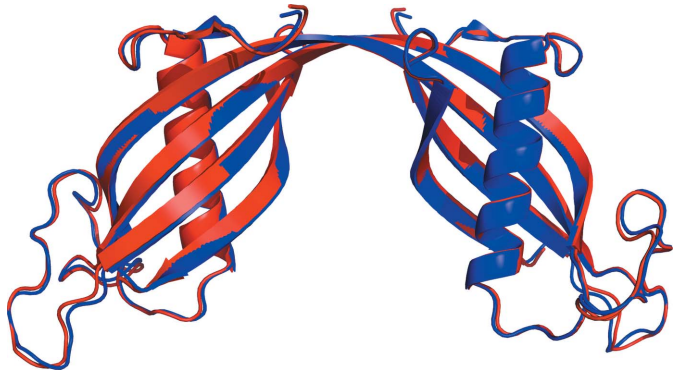

Figure 1
Superposition of the crystal structures of the domain-swapped dimeric hCC V57P (blue) and hCC V57D (red).

crystal structures have been determined [chicken cystatin (PDB entry 1cew; Bode *et al.*, 1988), dimeric hCC wt (PDB entry 1g96; Janowski *et al.*, 2001), hCC-stab1 (PDB entry 3gax; Kołodziejczyk *et al.*, 2010) and hCC V57N (PDB entry 3nx0; Orlikowska, Jankowska, Kolodziejczyk *et al.*, 2011)], no electron density was observed for the first nine residues of both mutants. The rest of the polypeptide chain for both proteins could be traced without ambiguity in the $2F_o - F_c$ map.

The secondary structure of hCC V57D and hCC V57P can be summarized as follows: (N)–β1–α–β2–βL–β3–(AS)–β4–L2–β5–(C), where AS is an 'appending structure' positioned at the opposite end of the β-sheet in relation to the inhibitory epitope. Both mutants are three-dimensional domain-swapped dimers with the (N)–β1–α–β2 motif serving as the swapping unit. The reciprocal character of this exchange leads to a highly symmetric dimeric molecule with two folding units positioned at an angle of about 100°. Each folding unit recreates the hCC wt monomer, the structure of which could be predicted based on the monomeric structures of the single-point V57N mutant of hCC (Orlikowska, Jankowska, Borek *et al.*, 2011) and the doubly mutated L47C/G69C hCC (hCC-stab1; Kołodziejczyk *et al.*, 2010). The L1 loop serves as a hinge element which adopts a different conformation during the domain-swapping process that converts the monomer to the dimeric structure. This loop, which is exposed in the monomer, becomes part of a long β-strand extending from the N-terminus of β2 to the C-terminus of β3 (Tyr42–Thr74). Two copies of this β-strand contributed by two hCC molecules participating in the swapping event face each other and create a long antiparallel β-hairpin stabilized by 30 (V57P) or 34 (V57D) hydrogen bonds. Most of the bonds between the β-strands mimic interactions that are present in the monomer. However, a few of the interactions that arise either from L1 loop opening or formation of the dimer-specific (βL) interface are exclusive to the domain-swapped dimer. Interatomic contacts formed by the βL residues (Supplementary Table S1[1]) may contribute to the increased stability of the dimeric form in comparison to the monomer.

3.3. The L1 loop

Comparison of the βL interface in the wild-type and the mutated hCC molecules explains how a substitution introduced at position 57 affects the architecture of the hinge region. The V57D mutation leaves the pattern of interactions in the β-hairpin virtually unchanged despite the significant difference in polarity and charge between valine and aspartic acid. The greater polarity of aspartic acid does not influence either the backbone disposition or the number of hydrogen bonds that stabilize the β-sheet structure in this region (Fig. 2). There are six interactions engaging the N and O backbone atoms from the Q^{55}IVAG fragment of each hCC molecule and they are the same in hCC wt and the V57D mutant (Supplementary Table S1). The V57P mutation has a more significant impact on the architecture of the βL interface. The rigidity of the cyclic side chain of proline affects the conformations of the subsequent amino acids, in particular Ala58 (Supplementary Table S2). The β-strands are forced apart, which creates an opening in the βL interface (Fig. 2). This conformational change results in a smaller number of hydrogen bonds stabilizing the βL area, which in the case of the V57P mutant decreases the number of hydrogen bonds in the Q^{55}IVAG fragment from six to only two.

3.4. Proline in position 57 and the dimerization propensity

Experiments with different proteins that undergo domain swapping revealed that changes in both the length of the hinge loop and the type of residues can affect the monomer–dimer equilibrium. Loop lengthening results in greater flexibility, slows the rate of folding into a monomeric structure and consequently increases the likelihood of the association of two unfolded chains into a domain-swapped dimer (Gordon-Smith *et al.*, 2001). The same destabilizing effect is observed in the shortened loops: deletions make the hinge chain too short to fold properly into a loop structure and draw the equilibrium towards the three-dimensional domain-swapped dimer or higher oligomer, in which the affected fragment can adopt an extended conformation (Ogihara *et al.*, 2001). The effect of mutations can be both stabilizing and destabilizing, and the results depend on the conformational strain introduced by the mutation. We expected that the V57P mutation would generate strain in the L1 loop and result in a greater propensity of the protein to unfold and oligomerize.

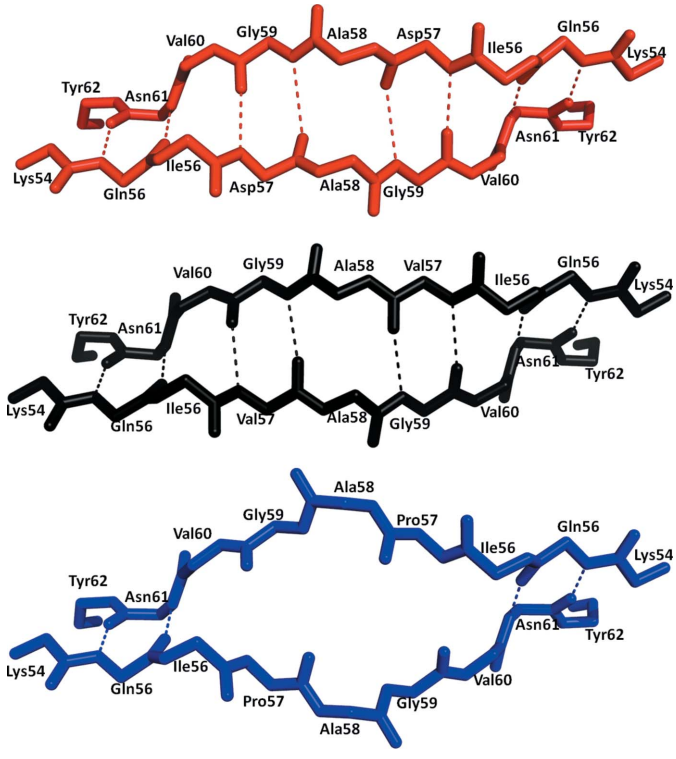

Figure 2
Hydrogen bonds stabilizing the βL interface in the dimeric molecules of V57D hCC (red), hCC wt (black) and V57P hCC (blue).

[1] Supplementary material has been deposited in the IUCr electronic archive (Reference: EN5523). Services for accessing this material are described at the back of the journal.

Experimental studies performed on the designed proteins confirmed that the V57P mutant is less stable in the folded monomeric form than any of the studied hCC variants. At a guanidine hydrochloride concentration of 0.5 *M*, which was routinely used to induce hCC dimerization, V57D and V57N remained mostly monomeric during the time of incubation, with 8.1% and 7.7% dimer fraction for V57D and V57N, respectively. The proline mutant was predominantly dimeric, even when freshly dissolved in the incubation buffer (Szymańska *et al.*, 2009).

The increased tendency of the V57P mutant towards dimerization/oligomerization may be related to the greater conformational flexibility of this mutant. We studied thermal and pressure-induced denaturation of hCC variants and the results of these studies consistently indicated V57P to be the least stable variant of hCC. Circular-dichroism experiments following heat-induced denaturation led to the determination of the melting point of the V57P mutant as being about 10 K lower than those of the V57N and V57D mutants (Fig. 3). This result clearly indicates that conformational changes in both α-helical (CD measurements at λ = 222 nm) and β-structural (λ = 218 nm) regions of the V57P molecule proceeded more easily than in the case of the hCC mutants with stabilizing substitutions at position 57. Hydrogen–deuterium exchange experiments following the impact of elevated pressure on the hCC variant structures showed a transition point for V57P at about 150 MPa, whereas this value was 300 MPa for hCC wt (Jankowska *et al.*, 2012). Also, the number of deuterons that were incorporated into the protein structure at ambient pressure was significantly greater for the V57P mutant compared with all other studied hCC variants. These observations indicate that the V57P mutant has the least stable structure and that which is most prone to unfolding. The unique conformational rigidity of proline probably plays a crucial role in the destabilization of the monomer, causing escalation of the backbone strain in the L1 loop region. The increased strain makes this loop act as a loaded molecular spring that relieves tension by adopting an extended conformation, which in turn induces partial unfolding of the protein molecule. The open monomer then exposes its hydrophobic interior to the solvent and this unfavourable transformation is most likely to induce the association of the unfolded chains

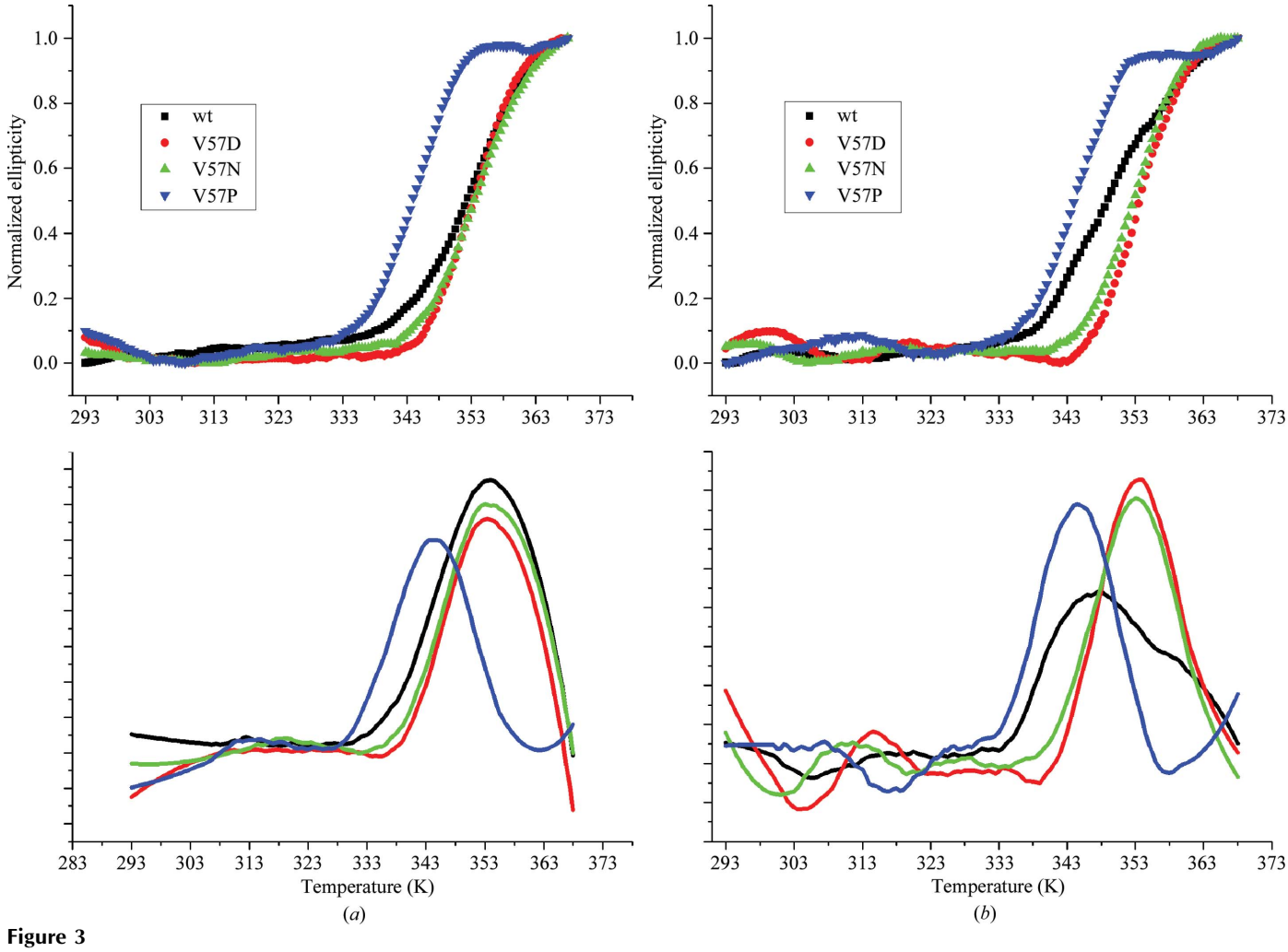

Figure 3
Thermal denaturation of hCC variants followed by circular-dichroism measurements at (*a*) λ = 218 nm and (*b*) λ = 222 nm. The upper charts present melting curves calculated on the basis of the recorded CD spectra; the lower charts present the first derivative of each melting curve smoothed using a 13-point Savitzky–Golay function.

into domain-swapped dimers as observed in the crystal structure. The architecture of the dimer is stabilized by 30 hydrogen bonds between the extended β-strands, and these interactions may make the V57P mutant sufficiently stable to crystallize in the dimeric form.

The electron density in the region of Pro57 is highly visible in the $2F_o - F_c$ map (Fig. 4), allowing the main and side chains to be traced without ambiguity. The proline residue in the obtained dimeric structure is in the *trans* conformation (Supplementary Table S2). Owing to the lack of an experimental structure of monomeric V57P, it is not possible to determine the conformation of Pro in the monomer. However, we cannot exclude the possibility that domain-swapping dimerization of the V57P mutant is facilitated by a proline *cis*→*trans* isomerization, which is known to play a role in the oligomerization of some proteins, including stefin B, a protein from the family I cystatins (Kokalj *et al.*, 2007).

3.5. Polar residues at position 57

We introduced Asn and Asp residues into position 57 to preserve the L1 loop structure and prevent hCC dimerization. Asparagine and aspartic acid can stabilize the conformations of turns and are frequently observed in turns. The previously obtained V57N mutant was a monomer not only in diluted solutions (Szymańska *et al.*, 2009), but also in the crystallization conditions (Orlikowska, Jankowska, Kolodziejczyk *et al.*, 2011). This result confirmed that the Asn residue can stabilize the hinge loop. We anticipated similar behaviour for the V57D hCC mutant, particularly because the equivalent mutant V55D of chicken cystatin remains monomeric under all conditions used to dimerize the wild-type protein (Staniforth *et al.*, 2001). Additionally, our studies of hCC stability using chemical (Szymańska *et al.*, 2009) and thermal denaturation demonstrated comparable stability of the native monomeric forms of both the V57N and the V57D mutants. However, the V57D mutant behaved differently during crystallization trials and did not crystallize in conditions identical to those which produced crystals in the case of V57N hCC (0.1 *M* cacodylate pH 6.5, 0.2 *M* ammonium sulfate, 25% PEG 8000). Crystals grown in a drop equilibrated against well solution consisting of 0.1 *M* imidazole pH 6.5, 1 *M* sodium acetate showed the V57D mutant structure as a domain-swapped dimer.

The most straightforward explanation for the different crystallization outcomes for the V57N and V57D mutants seems to be the different properties of Asn and Asp residues. While the side chain of asparagine is polar, aspartic acid is not only polar but also charged over a broad range of conditions. The pK_a for the side-chain carboxyl group of Asp is 3.9. Above this value the carboxyl group is ionized, so in the crystallization solution at pH 6.5 the Asp residue in the V57D mutant will have taken on the form of a carboxylate ion. The presence of a charged residue in the hydrophobic core can have a destabilizing effect by inducing repulsion and resulting in the exclusion of a β-sheet from the hydrophobic patches. This explanation would suggest that the Asp residue is better accommodated in the solvent-exposed L1 loop structure and would support our expectations about the monomeric arrangement of the V57D hCC mutant. However, the protein crystallized as a dimer (and also at pH 4.6; results not shown), indicating that the negative charge carried by the Asp residue does not destabilize the β-hairpin. Detailed analysis of the V57D mutant structure revealed that the side chain of Asp57 protrudes from the hydrophobic core of the βL interface (Fig. 5); for this reason, there are no unfavourable interactions that might disturb this interface. On the other hand, the charged residue in the hinge loop can influence a pattern of solvent interactions in the V57D monomer and thereby influence the dynamic properties of the whole protein. Increased conformational dynamics may result in transient unfolding of the protein and lead to domain swapping. Additionally, the V57D mutant may form the dimeric structure owing to the enthalpic gain resulting from favourable contacts of the Asp residue with the solvent molecules both in the unfolded open monomer and in the dimer. Interactions between the solvent molecules and the carboxylate group projecting outwards may compensate for the unfavourable

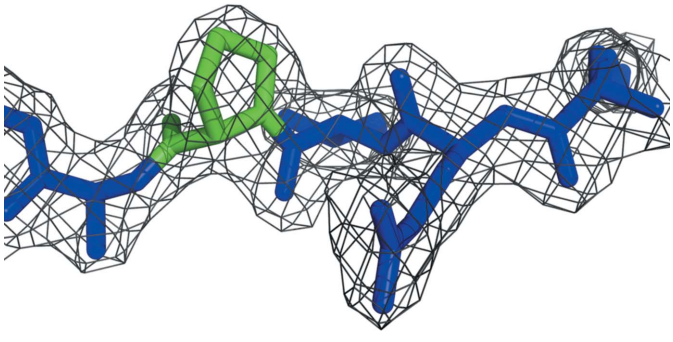

Figure 4
Fitting of the amino-acid residues from the unfolded L1 loop of the V57P mutant into electron density. The $2F_o - F_c$ electron-density map is contoured at the 1σ level.

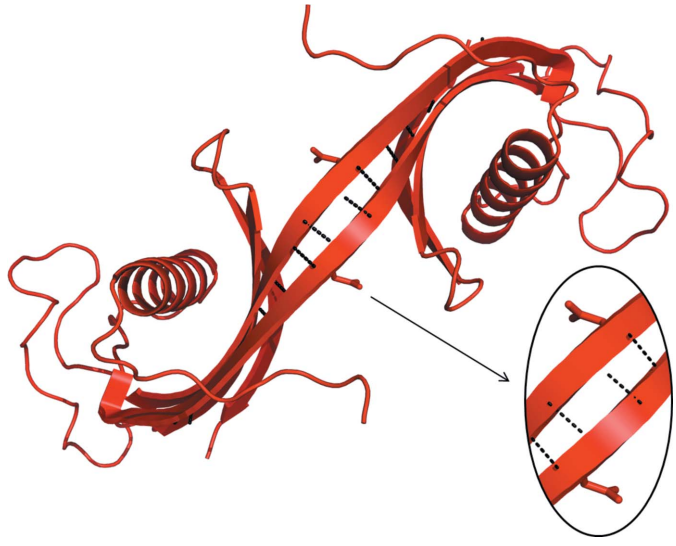

Figure 5
Asp57 residues protruding from the βL interface of the dimeric structure of V57D hCC.

contacts that result from a newly exposed hydrophobic interface in the transiently unfolded protein, stabilizing it for sufficiently long to facilitate protein dimerization. In the case of the V57N mutant, this stabilization could be less effective and insufficient to overcome the loop-stabilizing effect of the Asn residue.

However, this interpretation does not explain why the dimer is a more favourable form of the V57D mutant in the crystallization conditions, whereas the protein persists as a monomer in solution. To be sure that this different behaviour is not a consequence of the solution content, we performed a test in which the samples were prepared in the same way as for the crystallization trials, that is by mixing an aqueous solution of the protein (10 mg ml^{-1}) with a solution consisting of 1.0 *M* sodium acetate, 0.1 *M* imidazole pH 6.5 in a 1:1 ratio. Such samples were incubated at room temperature and analyzed at different time points by size-exclusion liquid chromatography. We found that after prolonged incubation of V57D hCC in conditions mimicking the crystallization reservoir the protein was still monomeric (data not shown). Thus, the dimerization of the V57D mutant during its crystallization does not seem to be a simple consequence of the crystallization conditions, but may rather be the result of specific interactions between the protein molecules and the surrounding solvent that change during equilibration of the system.

Our hydrogen–deuterium exchange pressure-induced denaturation studies also distinguished the V57D and V57N mutants as behaving differently under elevated pressure (Jankowska *et al.*, 2012). The mutant with aspartic acid at position 57 unfolded more easily and displayed a transition point at about 100 MPa lower than the V57N analogue. Concomitantly, however, the V57D variant refolded quickly after pressure relief, capturing a similar number of deuterons as V57N in its interior, and these numbers were higher than those measured for V57P and even hCC wt. Since pressure denaturation is connected with the penetration of solvent molecules into the interior of the protein, it may reveal different aspects of the protein–solvent interactions than the chemical or thermal denaturation defined as the exposure of the protein hydrophobic core to the solvent. It seems that these particular aspects became more important during crystallization of the V57D mutant.

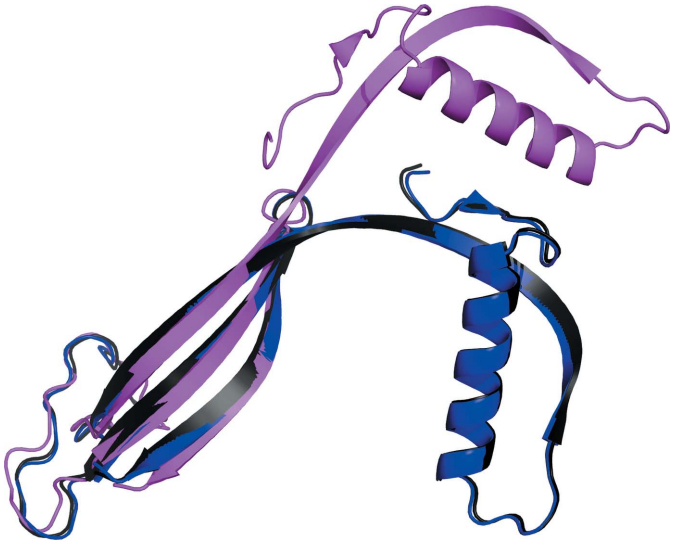

Figure 6
Structural alignment of the experimental structure of hCC V57P (blue) with the folding unit of three-dimensional domain-swapped hCC molecules: PDB entries 1g96 (Janowski *et al.*, 2001; black) and 1tij (Janowski *et al.*, 2005; magenta).

3.6. Comparison with other cystatin models

Superposition of the V57D or V57P mutant on wild-type hCC indicates that the mutation introduced at position 57 leaves the structures of the two monomer-like domains in the domain-swapped dimer virtually unchanged. The overall fold of hCC V57D and V57P also shows no significant differences when compared with the model of the domain-swapped dimer of hCC (PDB entry 1g96; Fig. 6), yielding r.m.s.d. deviation values of 0.42 and 0.61 Å for pairwise C$^{\alpha}$ superpositions of wild-type hCC on the V57D and V57P mutants, respectively (Supplementary Table S3). The tetragonal form of full-length human cystatin C (PDB entry 1tij; Janowski *et al.*, 2005) shows very significant deviations from the hCC V57D and V57P structures, with r.m.s.d. values of 5.46 and 5.39 Å, respectively. However, the internal organization of the monomer-like subdomains remains unchanged and the high r.m.s.d. values are a consequence of the different mutual orientation of the two cystatin-like folding units (Fig. 6). The β-strands creating each folding unit of the 1tij dimer are roughly parallel, running from one domain to the other in a straight fashion. In the V57D and V57P structures the linker region in the open interface has a curved shape, positioning the β-strands at an angle of about 100°, as in the case of 1g96. The results of least-squares superpositions of hCC V57D and V57P molecules with other cystatin models are summarized in Supplementary Table S3.

3.7. Crystal packing

The crystal structures of hCC mutants presented here are almost identical to the cubic form of wild-type human cystatin C (PDB entry 1g96). The solvent content is also approximately the same: for the V57D and V57P mutants it is about 71.5%, which is also the level obtained for 1g96 (Jaskólski, 2001). Therefore, it is not surprising that the packing interactions within the crystals of the mutated and wild-type proteins also do not change much. Four domain-swapped dimers of each hCC variant create octameric assemblies through a rich network of interactions with symmetry-related molecules. The connectivity within the sphere-like octamer is both dimeric and circular. In the wild-type hCC, nine unique hydrogen bonds in eight copies cement the dimers within the octamer together (Jaskólski, 2001). In the V57P mutant, ten such unique interactions can be identified. Among them, two hydrogen bonds are formed between α-helix residues from neighbouring dimers. Another three interactions involve the unstructured region between α1 and β2 of one dimer and β3, β5 or AS of the other. The remaining five contacts engage the

appending structure of one dimer, while the complementary hydrogen-bond donors/acceptors are located on the solvent-accessible surface of the β-sheet of the adjacent dimeric molecule. In the case of the V57D hCC mutant, which displays the same crystal packing, hydrogen bonds between the dimers within the octamer also involve mainly the convex surface of the C-terminal β-sheet and the so-called 'back-side loop' located on the opposite face of the molecule with respect to the inhibitory epitope.

Interactions between the octamers complete the connectivity pattern visible in the crystal lattice. The octamers interact with each other through van der Waals contacts involving the side chains of the Ile56, Ala58 and Val60 residues in the hinge loop. Although the position of some of these side chains is slightly different in particular hCC variants, all of the interactions that are visible between the octamers of hCC wt are present in the crystals of the mutated proteins. Thus, despite the fact that the Val57→Asp mutation introduced a huge difference in the hydrophobicity of the interacting region, it does not perturb the contacts between the octamers, presumably because the side chain of aspartic acid is not exposed to the surface of the octamer (Fig. 7).

To verify the relevance of the octameric assemblies observed in the crystals to the solution state, we utilized the *PISA* server (Krissinel & Henrick, 2007). For every studied hCC variant, an octamer was indicated by *PISA* to be the most stable form of the protein. Additionally, the free energy of dissociation of the octameric assemblies calculated by the *PISA* server confirms our predictions about the lower stability of the V57P mutant. The dissociation energy for this hCC variant was 24.7 kcal mol^{-1}, while for wild-type cystatin C (PDB entries 1g96 and 1r4c) and the V57D mutant it was about 6–8 kcal mol^{-1} greater (Table 2). It seems that the flexibility of the V57P molecule destabilizes every form of the protein: the monomer, the dimer and also the octamer.

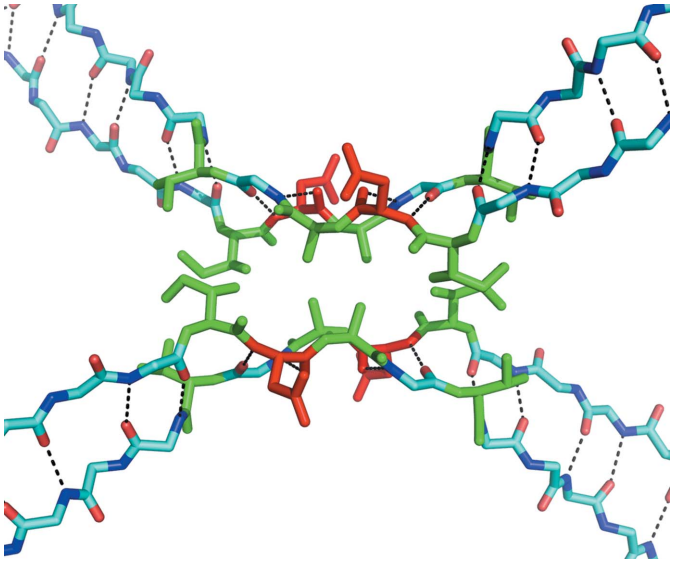

Figure 7
Hydrophobic interface between the two octamers of the V57D mutant in the crystal lattice. The interacting residues Ile56, Ala58 and Val60 are highlighted in green. Asp57 residues are marked in red.

Table 2
Results of calculations of the stability of octameric assemblies for crystal structures of different hCC variants using the *PISA* server (Krissinel & Henrick, 2007).

All ligands (polyethylene glycol and glycerol molecules and acetate ions) were excluded from calculations, as suggested by E. Krissinel (personal communication). PDB codes: 3s67, V57P hCC; 3sva, V57D hCC; 1g96, twofold-symmetric three-dimensional domain-swapped dimer (Janowski *et al.*, 2001); 1r4c, dimeric form of N-truncated hCC (Janowski *et al.*, 2004).

PDB code	Formula	Surface area (Å^2)	Buried area (Å^2)	$\Delta G^{\rm int}$ (kcal mol^{-1})	$\Delta G^{\rm diss}$ (kcal mol^{-1})
3s67	A_8	42360	37860	−190.4	24.7
3sva	A_8	40900	37440	−192.1	30.3
1g96	A_8	41120	37760	−175.4	31.5
1r4c	A_8	40600	38700	−192.6	32.9

4. Conclusions

In this paper, we have studied the role of the conformational strain imposed by residue 57 in the L1 loop in the regulation of the domain-swapping dimerization of hCC. Two mutated hCC variants have been obtained in which the wild-type Val57 has been replaced either by aspartic acid, which is favoured in β-turn structures, or proline, which broadens and destabilizes structural turns. The hCC V57D mutant, although stable in a monomeric form in solution, is a dimer in the crystal lattice. In this case, two phenomena may account, together or separately, for the shift of the equilibrium toward the dimeric form: firstly, increased conformational dynamics of the monomer and, secondly, stabilization of the unfolded conformation of the monomer by interactions with solvent molecules. The hCC V57P mutant was obtained as a dimer in crystals, but this mutant also displayed a propensity for higher oligomerization. The proline residue influenced the conformation of the βL interface, diminishing the number of hydrogen bonds that stabilize it.

This work was supported in part by the Polish Ministry of Science and Higher Education 2739/B/H03/2010/38 and by grant DS/8440-4-0172-2.

References

Barrett, A. J. (1987). *Trends Biochem. Sci.* **12**, 193–196.
Bennett, M. J., Choe, S. & Eisenberg, D. (1994). *Proc. Natl Acad. Sci. USA*, **91**, 3127–3131.
Bennett, M. J., Schlunegger, M. P. & Eisenberg, D. (1995). *Protein Sci.* **4**, 2455–2468.
Bode, W., Engh, R., Musil, D., Thiele, U., Huber, R., Karshikov, A., Brzin, J., Kos, J. & Turk, V. (1988). *EMBO J.* **7**, 2593–2599.
Brünger, A. T. (1992). *Nature (London)*, **355**, 472–475.
Chen, V. B., Arendall, W. B., Headd, J. J., Keedy, D. A., Immormino, R. M., Kapral, G. J., Murray, L. W., Richardson, J. S. & Richardson, D. C. (2010). *Acta Cryst.* D**66**, 12–21.
Chiti, F. & Dobson, C. M. (2006). *Annu. Rev. Biochem.* **75**, 333–366.
Crestfield, A. M., Stein, W. H. & Moore, S. (1962). *Arch. Biochem. Biophys.*, Suppl. 1, 217–222.
Dehouck, Y., Biot, C., Gilis, D., Kwasigroch, J. M. & Rooman, M. (2003). *J. Mol. Biol.* **330**, 1215–1225.

Ekiel, I. & Abrahamson, M. (1996). *J. Biol. Chem.* **271**, 1314–1321.
Emsley, P. & Cowtan, K. (2004). *Acta Cryst.* D**60**, 2126–2132.
Engh, R. A., Dieckmann, T., Bode, W., Auerswald, E. A., Turk, V., Huber, R. & Oschkinat, H. (1993). *J. Mol. Biol.* **234**, 1060–1069.
Gille, C. & Frömmel, C. (2001). *Bioinformatics*, **17**, 377–378.
Gordon-Smith, D. J., Carbajo, R. J., Stott, K. & Neuhaus, D. (2001). *Biochem. Biophys. Res. Commun.* **280**, 855–860.
Jankowska, E., Stefanowicz, P., Sosnowska, M., Karpowicz, P., Radziszewska, K., Szewczuk, Z. & Szymańska, A. (2012). *Proteins*, **80**, 2417–2425.
Janowski, R., Abrahamson, M., Grubb, A. & Jaskolski, M. (2004). *J. Mol. Biol.* **341**, 151–160.
Janowski, R., Kozak, M., Abrahamson, M., Grubb, A. & Jaskolski, M. (2005). *Proteins*, **61**, 570–578.
Janowski, R., Kozak, M., Jankowska, E., Grzonka, Z., Grubb, A., Abrahamson, M. & Jaskolski, M. (2001). *Nature Struct. Biol.* **8**, 316–320.
Jaskólski, M. (2001). *Acta Biochim. Pol.* **48**, 807–827.
Jenko Kokalj, S., Guncar, G., Stern, I., Morgan, G., Rabzelj, S., Kenig, M., Staniforth, R. A., Waltho, J. P., Zerovnik, E. & Turk, D. (2007). *J. Mol. Biol.* **366**, 1569–1579.
Kołodziejczyk, R., Michalska, K., Hernandez-Santoyo, A., Wahlbom, M., Grubb, A. & Jaskolski, M. (2010). *FEBS J.* **277**, 1726–1737.
Krissinel, E. & Henrick, K. (2007). *J. Mol. Biol.* **372**, 774–797.
Laskowski, R. A., MacArthur, M. W., Moss, D. S. & Thornton, J. M. (1993). *J. Appl. Cryst.* **26**, 283–291.
Liu, C., Sawaya, M. R. & Eisenberg, D. (2011). *Nature Struct. Mol. Biol.* **18**, 49–55.
Liu, Y. & Eisenberg, D. (2002). *Protein Sci.* **11**, 1285–1299.
Martin, J. R., Craven, C. J., Jerala, R., Kroon-Zitko, L., Zerovnik, E., Turk, V. & Waltho, J. P. (1995). *J. Mol. Biol.* **246**, 331–343.
Minor, W., Cymborowski, M., Otwinowski, Z. & Chruszcz, M. (2006). *Acta Cryst.* D**62**, 859–866.
Murshudov, G. N., Skubák, P., Lebedev, A. A., Pannu, N. S., Steiner, R. A., Nicholls, R. A., Winn, M. D., Long, F. & Vagin, A. A. (2011). *Acta Cryst.* D**67**, 355–367.
Nilsson, M., Wang, X., Rodziewicz-Motowidlo, S., Janowski, R., Lindström, V., Onnerfjord, P., Westermark, G., Grzonka, Z., Jaskolski, M. & Grubb, A. (2004). *J. Biol. Chem.* **279**, 24236–24245.
Ogihara, N. L., Ghirlanda, G., Bryson, J. W., Gingery, M., DeGrado, W. F. & Eisenberg, D. (2001). *Proc. Natl Acad. Sci. USA*, **98**, 1404–1409.
Olafsson, I. & Grubb, A. (2000). *Amyloid*, **7**, 70–79.
Orlikowska, M., Jankowska, E., Borek, D., Otwinowski, Z., Skowron, P. & Szymańska, A. (2011). *Acta Cryst.* F**67**, 1608–1611.
Orlikowska, M., Jankowska, E., Kolodziejczyk, R., Jaskólski, M. & Szymańska, A. (2011). *J. Struct. Biol.* **173**, 406–413.
Otwinowski, Z. & Minor, W. (1997). *Methods Enzymol.* **276**, 307–326.
Painter, J. & Merritt, E. A. (2006*a*). *J. Appl. Cryst.* **39**, 109–111.
Painter, J. & Merritt, E. A. (2006*b*). *Acta Cryst.* D**62**, 439–450.
Rodziewicz-Motowidło, S., Iwaszkiewicz, J., Sosnowska, R., Czaplewska, P., Sobolewski, E., Szymańska, A., Stachowiak, K. & Liwo, A. (2009). *Biopolymers*, **91**, 373–383.
Rousseau, F., Schymkowitz, J. W., Wilkinson, H. R. & Itzhaki, L. S. (2001). *Proc. Natl Acad. Sci. USA*, **98**, 5596–5601.
Sastre, M., Calero, M., Pawlik, M., Mathews, P. M., Kumar, A., Danilov, V., Schmidt, S. D., Nixon, R. A., Frangione, B. & Levy, E. (2004). *Neurobiol. Aging*, **25**, 1033–1043.
Shameer, K., Shingate, P. N., Manjunath, S. C. P., Karthika, M., Pugalenthi, G. & Sowdhamini, S. (2011). *Database*, **2011**, bar042.
Staniforth, R. A., Giannini, S., Higgins, L. D., Conroy, M. J., Hounslow, A. M., Jerala, R., Craven, C. J. & Waltho, J. P. (2001). *EMBO J.* **20**, 4774–4781.
Szymańska, A., Jankowska, E., Orlikowska, M., Behrendt, I., Czaplewska, P. & Rodziewicz-Motowidło, S. (2012). *Frontiers Mol. Neurosci.* **5**, 82.
Szymańska, A., Juszczyk, P., Jankowska, E., Radulska, A., Wahlbom, M., Grubb, A., Liberek, K. & Rodziewicz-Motowidło, S. (2008). *Peptides 2008. Chemistry of Peptides in Life Science, Technology and Medicine. Proceedings of the 30th European Peptide Symposium*, edited by H. Lankinen, pp. 630–631. Helsinki: The Finnish Peptide Society.
Szymańska, A., Radulska, A., Czaplewska, P., Grubb, A., Grzonka, Z. & Rodziewicz-Motowidło, S. (2009). *Acta Biochim. Pol.* **56**, 455–463.
Vagin, A. & Teplyakov, A. (2010). *Acta Cryst.* D**66**, 22–25.
Winn, M. D. *et al.* (2011). *Acta Cryst.* D**67**, 235–242.
Žerovnik, E., Stoka, V., Mirtič, A., Gunčar, G., Grdadolnik, J., Staniforth, R. A., Turk, D. & Turk, V. (2011). *FEBS J.* **278**, 2263–2282.
Zhang, Y. & Skolnick, J. (2005). *Nucleic Acids Res.* **33**, 2302–2309.